BL-6A/2021G040

Stress Response and Deformation of Block Copolymers with Single-Crystal-Like Lamellar Structures: Effect of the Lateral Size of Lamellae

Masatoshi TOKITA[1]*

[1] Department of Chemical Science and Engineering, Tokyo Institute of Technology, Ookayama, Meguro, Tokyo 152-8550, Japan

1 Introduction

Semicrystalline polymers form lamellar structures comprising alternating stacks of crystalline and amorphous layers at a 10-nm spacing. Deformation of semicrystalline polymers involving the deformation of structures has been extensively examined for semicrystalline polymers due to industrial incentives to explain processes associated with crystal orientation by drawing and spinning [1–3]. However, the relationship between the lamellar deformation and the stress response cannot be clearly related to each other. The lamellar deformation mechanism depends on the angle between the lamellar stacking and deformation directions. In viewing polymer crystals on a micrometer scale, the lamellae radiate from a point to an assemblage of 1-μm sized spherulite. In a tensile-deformed spherulite, lamellae stacking in the tensile direction undulate and bend at localized hinges to form the chevron structure as the strain increases. However, the other lamellae, which stack in the direction inclined to the tensile direction, slip or rotate to be parallel to the stretching direction.[4] Thus, all lamellae do not undergo the same deformation under macroscopic deformations.

Clarifying the relationship between the lamellar deformation and the stress response requires uniform deformation of microstructure and samples with globally arranged microstructures, like single crystals. Single crystal-like microstructural samples have been prepared for block copolymers (BCPs). Single-crystal-like films of BCP lamellae were cut from large-grained films prepared by roll casting of poly(styrene) (PS)–poly(butadiene) (PB)–PS BCPs [5–7], and the lamellar deformation and stress response were examined [8,9]. We have found a straightforward method for preparing similar single crystal-like microlamellar samples using a series of liquid crystal (LC) BCPs (LC BCPs). These LC BCPs, designated as B5-*x*-EMA-*φ*, comprise a main-chain smectic LC BB-5(3-Me) polyester bonded at both ends to poly(ethyl methacrylate) (PEMA) segments (Fig. 1) [10–16]. *x* and *φ* are the number average molecular weight of the BB-5(3-Me) segment ($M_{n,LC}$) in units of kDa and the PEMA segment volume percentage, respectively (see Table 1 for details). Characteristically, B5-*x*-EMA-*φ* forms lamellar microdomains at *φ* in a relatively wide range of 20%–50%. Moreover, these microdomain lamellae are stacked along the film length direction when the films are drawn from the copolymer melt, with both segments in the liquid state, and subsequently annealed at a lower temperature where the LC segment is in the smectic LC phase.

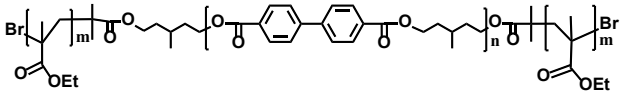

Fig. 1: Chemical structure of B5-*x*-EMA-*φ*.

Herein, we report the effects of lamellar lateral dimensions on the stress response and structural deformation on stretching lamellae along the normal direction. Lamellae having limited lateral size (short lamellae) are characteristically formed by B5-*x*-EMA-*φ* at greater φ [13,15,16]. Two B5-*x*-EMA-*φ* copolymers of B5-29-EMA-22 and B5-29-EMA-44 were prepared, with the same *x* and different *φ*. B5-29-EMA-22 forms long-range continuous lamellae, whereas B5-29-EMA-44 forms short lamellae comprising LC block lamellae separated by PEMA segments. Single crystal-like lamellar films of these copolymers were prepared and stretched in the lamellar normal direction to measure the stress–elongation (*σ*–*λ*) curves. The curves overlap in the initial elastic region but separate in the region beyond the yield point. B5-29-EMA-22 shows a stress plateau accompanying the microstructural transformation of undulating and folding lamellae, forming a chevron structure. In contrast, B5-29-EMA-44 increases the stress following the yielding (strain hardening). This strain hardening involves an increase in the lamellar spacing without tilting. We assume that this strain hardening is characteristic of short lamellae.

2 Experiment

Materials: B5-29-EMA-22 and B5-29-EMA-44 copolymers were prepared by atom transfer radical polymerization of ethyl methacrylate using a macroinitiator prepared from a BB-5(3-Me) polyester by changing the monomer feed ratio [13,15]. The polydispersity indices of these copolymers were 1.6–1.7 as determined by size-exclusion chromatography calibrated using the polystyrene standards. BB-5(3-Me) segments formed a smectic CA liquid crystal which displayed the glass transition at 30°C and transformed to the isotropic liquid at 150 °C. The glass transition temperature (T_g) of the PEMA measured for homo PEMA was 70 °C, although the T_g of the PEMA block was barely detected, likely due to the smaller PEMA fraction in the copolymer.

Methods: Synchrotron radiation small-angle X-ray scattering (SAXS) measurements were performed at the BL-6A beamline at Photon Factory, Tsukuba, Japan, using a Dectris Pilatus3 1M detector [17]. The X-ray radiation wavelength (λ_X) and sample-to-detector distance were 0.15 nm and 2.5 m, respectively. A film sample at 100 °C was continuously stretched using a Linkam TST350 tensile stage at a crosshead speed of 1.3 μm s^{-1} (nominal strain rate 5% min^{-1}). The test sample length and cross-sectional dimensions were 1.5 mm and 0.6 × 0.02 mm, respectively. The X-ray scattering patterns were recorded at an exposure time of 30 s. The scattering intensity was presented as a function of the scattering vector $q = 4\pi \sin\theta/\lambda_X$, where 2θ is the scattering angle. Wide-angle X-ray diffraction (WAXD) measurements were conducted using a Bruker D8 DISCOVER equipped with a Cu-Kα radiation source and a Vantec-500 detector.

3 Results and Discussion

Lamellar Microstructures. The microstructures of the films prepared by pulling the cast films at 180 °C and subsequent annealing for 6 h at 120 °C were investigated. For both copolymers, the LC segment segregates from the PEMA segments to form 2-nm spaced smectic LC layers and lamellar microdomains at a spacing in the order of 10 nm [10,12–16]. The WAXD patterns revealed the structure and orientation of the smectic layers. The patterns include sharp reflections in the vertical direction parallel to the film length direction, indicating the smectic layers stacked up arranging their normal parallel the film length direction (Fig. 2a). The layer spacing is estimated to be 1.63 nm from the smallest angle reflection. The pattern also has a pair of diffuse reflections (halos) with a d-spacing of 0.45 nm at a larger diffraction angle in the direction orthogonal to the film length direction. These halos have intensity maxima above and below the equatorial line, indicating that mesogens' long axes are tilted from the layer normal. These reflections are characteristic to the smectic CA structure formed by main-chain LC polymers [18]. The same B5-29-EMA-22 sample displayed a SAXS pattern including two scattering maxima at q = 0.2 and 0.4 nm^{-1} located on the meridional line (Fig. 2b). These maxima are ascribed to the lamellar microdomains stacked at a 30-nm spacing along with the film length direction. Combining these WAXD and SAXS patterns allows depicting the hierarchical layer structures comprising 30-nm spaced two-phase microdomain lamellae (Fig. 2d). The two phases are smectic LC and amorphous. The smectic LC phase consists of the BB-5(3-Me) segment and forms smectic layers lying parallel to the lamellar microdomain interface and stacked at a spacing of 1.63 nm.

B5-29-EMA-44 is similar to B5-29-EMA-22 in the hieratical lamellar structure, but the stacked microdomain lamellae have smaller lateral dimensions than B5-29-EMA-22. The SAXS pattern of B5-29-EMA-44 is similar to that of B5-29-EMA-22 in several reflections at q with integer ratios in the fiber axis direction; however, the pattern is different in the shape of the reflections: the reflections are more elongated in the horizontal direction than that of B5-29-EMA-22. Such reflection shapes are associated with the stacking of small-dimensioned lamellae [19]. Indeed, lamellae with smaller lateral dimensions can be found on electron microscopy images of B5-29-EMA-44 (not shown here). Such lamellar separation has been observed for homologous LC BCPs having greater molecular-weight PEMA segments [13,15,16]. B5-29-EMA-44 forms short lamellae of the LC block and produces film samples with the lamellae stacked up along the length direction.

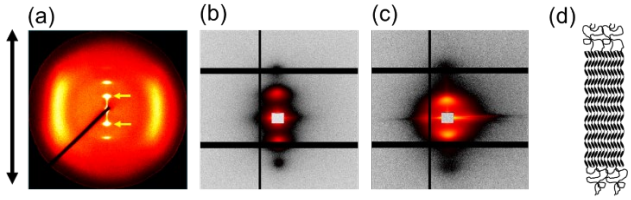

Fig. 2: (a) WAXD and (b) SAXS patterns measured for B5-29-EMA-22. (c) SAXS pattern of B5-29-EMA-44. (d) Schematic of B5-29-EMA-φ microstructure made by combining WAXD and SAXS patterns. The black arrow indicates the film length direction. The yellow arrows in (a) point to the smectic layer reflection with a d-spacing of 1.63 nm.

Stress–Elongation Curves. Figure 3 shows the stress–elongation curves of the copolymer film samples elongated in the film length direction (i.e., the stacking direction of microdomain lamellae). The curve of B5-29-EMA-22 is similar to that measured for B5-26-EMA-41 in a previous study [14]. As the extension ratio (λ) increases, the nominal tensile stress (σ) increases and culminates to 0.95 MPa at λ = 1.15, then remains constant at a value of 0.75 MPa at λ-value of up to 3. The curve of B5-29-EMA-44 almost overlaps with that of B5-29-EMA-22 in the initial region at $\lambda < 1.15$; however, on further increasing λ, σ increases continuously to show strain hardening. In both cases, increasing the λ-value above 3 decreases the force, makes the samples thinner and causes breaking. These results demonstrate that the σ–λ curve of the B5-29-EMA-φ copolymer is affected by the lamellar lateral dimensions. The stress hardening following the yielding can be associated with the divided lamellar morphology of B5-29-EMA-44.

Microstructural Deformations. Simultaneously with the σ–λ curves, SAXS images were measured using a synchrotron radiation X-ray source, and the representative images are shown in Fig. 4. The images of B5-29-EMA-22 shown in Fig. 4a–e are similar to those measured for B5-26-EMA-41 in the previous study [14]. When λ increases to 1.1, the meridional peak position shifts toward smaller q values. When λ increases to 1.5, the peaks spread in the azimuthal direction, suggesting the undulation of the lamellae. When λ further increases to 2.0, the reflections split to display a four-point pattern, ascribed to a chevron structure, consisting of predominantly straight layers, but bent at localized hinge regions. When λ reaches 2.4, the four-point reflections displace further from the meridional direction, and each reflection is off from the meridian by an angle as large as 80°. In contrast, the stretched B5-29-

EMA-44 samples always displayed SAXS maxima on the meridional line (Fig. 4f–j). The scattering maxima moved toward smaller q values as λ increases. These patterns demonstrate that the macroscopic deformation of B5-29-EMA-44 merely increases the lamellar spacing.

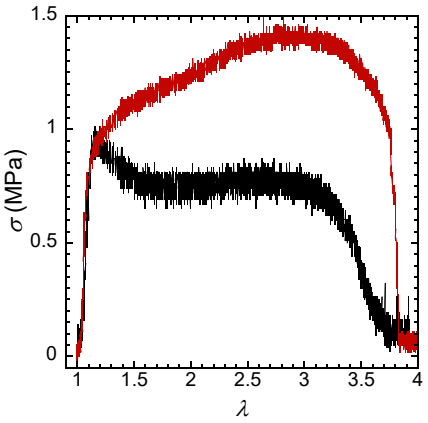

Fig. 3: σ–λ curves measured for B5-29-EMA-22 (black line) and B5-29-EMA-44 (red line).

To treat the lamellar deformations quantitatively, the lamellar spacing d_0 and the average tilt angle of the lamellae to the elongation direction θ_{LAM} were measured using the SAXS patterns, and the values are plotted against λ in Fig. 5. θ_{LAM} was determined from the azimuthal angle measured from the meridional line (film length direction) for the four-point SAXS patterns. For the SAXS pattern including azimuthally spread peaks, θ_{LAM} was assumed to be equal with the half-width at half-maximum (HWHM) of the azimuthal scans of the first-order reflection [9,14]. For B5-29-EMA-22, d increases from 31 to 44 nm as λ increases to 1.7, and then it recovers, albeit further λ increment. θ_{LAM} increases slightly from 20° to 26° as λ increases to 1.7 and jumps to 49° at λ = 1.8. This jump in θ_{LAM} corresponds to the appearance of the four-point SAXS pattern. In the σ–λ curve, λ = 1.7 is the starting point of the stress plateau following the stress maximum (see Fig. 4). These results indicate that as λ increases, the strain energy applied to stack the lamellae in the normal direction increases the spacing and rotates or tilts the normal direction away from the elongation direction. In contrast, for B5-29-EMA-44, the applied strain energy only increases d. The film deformation widens the SAXS peaks horizontally rather than arcuately and shifts the scattering peaks location at a smaller q. The film elongation increases the lamellar spacing without tilting lamellae. The lamellar spacing will increase continuously with increasing λ; however, SAXS cannot follow up the increase in d at λ > 2.0 because the lamellar reflection shifted toward smaller q values over the resolution of the SAXS setup.

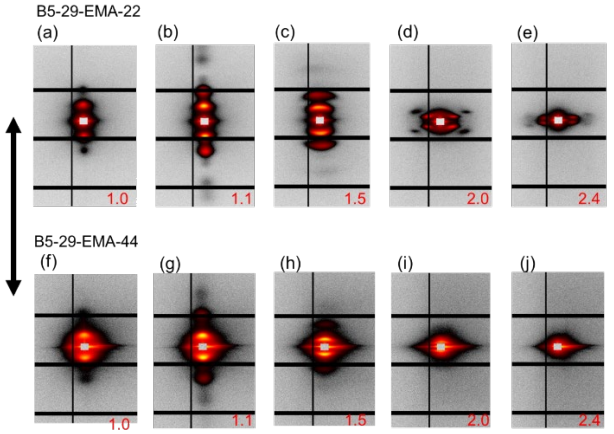

Fig. 4: SAXS patterns measured during deformation of (a–e) B5-29-EMA-22 and (f–j) B5-29-EMA-44 films at 120 °C, with load applied parallel to the lamellar normal at λ indicated at the lower right in each image. The tensile direction is vertical.

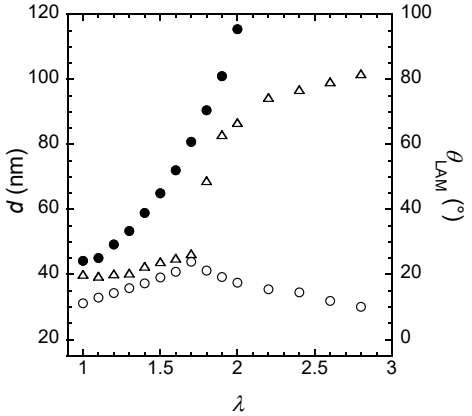

Fig. 5: Changes in lamellar spacing d (circle), and tilt angle θ_{LAM} (triangle) for B5-29-EMA-22 (open marks) and B5-29-EMA-44 (closed marks). For B5-29-EMA-44, the tilting of lamellae is not confirmed and the θ_{LAM} is not plotted.

Here we will examine the relationship between these microscopic lamellar dilations and rotations and the macroscopic sample deformation [9,14]. According to the affine dilation/tilting model [8], the sample length L is equal to Nd_z, where N is the number of lamellae stacked along the stretching direction, and d_z is the repeat length of the lamellae along the stretching direction. $d_z = d$ when the lamellae maintain the normal direction in the sample length direction, as in B5-29-EMA-44, whereas tilted (or rotated) lamellae have $d_z = d/\cos\theta_{LAM}$. The agreement between the measured microscopic and macroscopic sample deformations was examined by plotting the ratio of d_z to the d_z of an undeformed sample ($d_{z,0}$) against λ (Fig. 6). At λ < 1.7, B5-29-EMA-44 shows good correspondences between $d_z/d_{z,0}$ and λ, whereas B5-29-EMA-22 has smaller d_z/d_0 values than λ in the same range, which can be attributed to an error in estimating θ_{LAM} from the HWHM of the arced lamellar reflection.

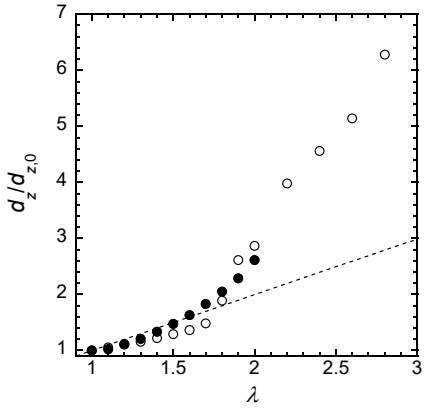

Fig. 6: Evaluation of affine dilation/tilting model for microdomain lamellae deformation in B5-29-EMA-22 (open mark) and B5-29-EMA-44 (closed mark) films.

At $\lambda > 1.7$, both copolymers exhibited $d_z/d_{z,0}$ values greater than λ, showing a remarkable deviation from the affine deformation. This non-affine microstructural deformation is ascribed to inhomogeneous lamellar deformations along the gauge length. The stretched film samples have their longer sides curved toward the centerline. The inhomogeneous lamellar deformations are confirmed with the SAXS patterns measured by irradiating a stretched copolymer film with the X-ray at the center with the narrowest width and at the end. A stretched B5-29-EMA-44 film more dilated the lamellar spacing at the center of rectangular film samples than at the end: the film stretched at $\lambda = 1.5$ showed $d = 59.0$ nm at the center, considerably exceeding $d = 51.4$ nm measured at the end of the film. A stretched B5-29-EMA-22 film more tilted the lamellae at the center: for the film elongated at $\lambda = 2.0$, d and θ_{LAM} were measured respectively to be 38.3 nm and 59°at the center, whereas that measured at the end were 44.5 nm and 22°. These differences in the values indicate that the film elongation deforms the microstructure preferentially at the center of the film specimen.

The results presented above show that lamellar lateral size affects the stress response and lamellar deformation on stretching in the normal direction. Between B5-29-EMA-22 and B5-29-EMA-44 forming respectively long and short lamellae, the stress responses are similar in the initial elastic increase, whereas further increasing λ makes the response different. B5-29-EMA-22 shows a maximum in σ, then drops σ and keeps a constant σ value. In contrast, B5-29-EMA-44 continues increasing σ, undergoing strain hardening. The tensile deformation of the copolymer film samples involves lamellar deformation. The lamellar deformation differs between these copolymers at strains beyond the yield point. The long lamellae in B5-29-EMA-22 are undulated and folded, forming chevrons. In contrast, the short lamellae in B5-29-EMA-44 are merely dilated to increase the spacing. Thus, the difference in the stress response can relate to the difference in the lamellar deformation. This strain hardening of B5-29-EMA-44 differs from that usually observed for solid polymers in the primary factor. This strain hardening cannot be attributed to the stress transfer through stretched chains. The PEMA segments are unlikely to be entangled, so the stress cannot be transmitted via the polymer chains. The molecular weight of the PEMA segment ($M_{n,am}/2$) is 10500, which is smaller than twice that of an entangled strand ($M_e = 6000$) evaluated from rheological measurements [20].

Acknowledgement

4,4′-dimethyl biphenyl dicarboxylate was kindly supplied by Ihara-nikkei Chemical Industry Co. Ltd. This work was supported by JSPS KAKENHI for Scientific Research on Innovative Areas “MFS Materials Science (Grant Number JP19H05120 and JP21H00095)”, and JSPS KAKENHI Grant Number JP19H02770.

References

[1] J. Che, C.R. Locker, S. Lee, G.C. Rutledge, B.S. Hsiao, and A.H. Tsou, *Macromolecules*, **46**, 5279 (2013).
[2] A. Rozanski and A. Galeski, *Macromolecules*, **48**, 5310 (2015).
[3] Z. Jiang, Y. Tang, Y. Men, H.-F. Enderle, D. Lilge, S. Roth, R. Gehrke, and J. Rieger, *Macromolecules*, **40**, 7263 (2007).
[4] M. Krumova, S. Henning, and G.H. Michler, *Phil. Mag.*, **86**, 1689 (2006).
[5] R.J. Albalak and E.L. Thomas, *J. Polym. Sci. B*, **31**, 37 (1993).
[6] R.J. Albalak, E.L. Thomas, and M.S. Capel, *Polymer*, **38**, 3819 (1997).
[7] M.A. Villar, D.R. Rueda, F. Ania, and E.L. Thomas, *Polymer*, **43**, 5139 (2002).
[8] Y. Cohen, R.J. Albalak, B.J. Dair, M.S. Capel, and E.L. Thomas, *Macromolecules*, **33**, 6502 (2000).
[9] Y. Cohen, M. Brinkmann, and E.L. Thomas, *J. Chem. Phys.*, **114**, 984 (2001).
[10] R. Ishige, T. Ishii, M. Tokita, M. Koga, S. Kang, and J. Watanabe, *Macromolecules*, **44**, 4586 (2011).
[11] M. Koga, M. Tokita, R. Ishige, K. Sato, T. Ishii, S. Kang, K. Sakajiri, J. Watanabe, M. Tokita, *Macromolecules*, **44**, 4586 (2012).
[12] M. Koga, K. Sato, S. Kang, K. Sakajiri, J. Watanabe, and M. Tokita, *Macromol. Chem. Phys.*, **214**, 2295 (2013).
[13] M. Hayashi, J. Kuribayashi, and M. Tokita, *Polymer*, **178**, 121555 (2019).
[14] J. Kuribayashi, R. Ishige, M. Hayashi, and M. Tokita, *Macromol. Chem. Phys.*, **221**, 1 (2020).
[15] M. Hayashi, J. Kuribayashi, and M. Tokita, *Polymer*, **211**, 123086 (2020).
[16] M. Koga, K. Abe, K. Sato, J. Koki, S. Kang, K. Sakajiri, J. Watanabe, and M. Tokita, *Macromolecules*, **47**, 4438 (2014).
[17] N. Shimizu, T. Mori, N. Igarashi, H. Ohta, Y. Nagatani, T. Kosuge, and K. Ito, *J. Phys.: Confer. Ser.*, **425**, (2013).
[18] K. Osada, M. Koike, H. Tagawa, M. Tokita, and J. Watanabe, *Macromol. Chem. Phys.*, **205**, 1051 (2004).
[19] N. Kasai and M. Kakudo, “X-Ray Diffraction by Macromolecules”, Springer Berlin Heidelberg, Berlin, Heidelberg (2005).
[20] J. Hrouz, M. Ilavský, J. Spěváček, and J. Trekoval, *Makromol. Chem.*, **181**, 277 (1980).

* tokita.m.aa@m.titech.ac.jp